Hindawi Publishing Corporation
International Journal of Geophysics
Volume 2012, Article ID 418084, 7 pages
doi:10.1155/2012/418084

Research Article

Entropy-Based Clutter Rejection for Intrawall Diagnostics

Raffaele Solimene and Antonietta D'Alterio

Dipartimento di Ingegneria dell'Informazione, Seconda Università degli Studi di Napoli, 81031 Aversa, Italy

Correspondence should be addressed to Raffaele Solimene, raffaele.solimene@unina2.it

Received 16 March 2012; Accepted 1 May 2012

Academic Editor: Francesco Soldovieri

The intrawall diagnostic problem of detecting localized inhomogeneities possibly present within the wall is addressed. As well known, clutter arising from masonry structure can impair detection of embedded scatterers due to high amplitude reflections that wall front face introduces. Moreover, internal multiple reflections also can make it difficult ground penetrating radar images (radargramms) interpretation. To counteract these drawbacks, a clutter rejection method, properly tailored on the wall features, is mandatory. To this end, here we employ a windowing strategy based on entropy measures of temporal traces "similarity." Accordingly, instants of time for which radargramms exhibit entropy values greater than a prescribed threshold are "silenced." Numerical results are presented in order to show the effectiveness of the entropy-based clutter rejection algorithm. Moreover, a comparison with the standard average trace subtraction is also included.

1. Introduction

Microwave RADAR imaging is a pervasive research field which finds applications in a number of scenarios where it is mandatory and/or convenient to achieve diagnostics in a nondestructive way. Applicative contexts range from subsurface prospecting to cultural heritage monitoring and preservation [1], from biomedical diagnostics [2] to through-the-wall imaging (TWI) [3], and many others.

Each one of these scenarios characterizes imaging in terms of the challenges to be tackled in order to succeed in target detection and localization. This of course depends on the scatterers' nature and the host medium within which they are embedded.

Indeed, the host medium is the background against which targets have to be discerned.

First, the host medium imposes a suitable trade-off between resolution and electromagnetic wave penetration in order to comply with losses and dispersive effects it introduces. Moreover, host medium also determines that clutter signal against field backscattered from targets must compete.

Literature is extremely reaches imaging algorithms arisen from different scientific areas. Now, it is recognized that wave equation is their common mathematical rationale. Accordingly, they all attempt to solve an electromagnetic inverse scattering problem by approximating, in different way, the inverse of the relevant scattering operator. The interested reader can refer to [4], where many of these imaging algorithms are compared under the light of inverse scattering theory.

In any case, imaging greatly benefits from a preliminary stage where useful signals (i.e., the ones coming from targets) are "singled out" from cluttered measurements.

Clutter embodies are all those unwanted field contributions which come from background medium heterogeneities and corrupt scattered field data. Indeed, clutter rejection methods are very much welcome as in most practical cases clutter has an amplitude dynamic range much greater than useful signals. The results is that targets tend to be masked and their detection can be strongly impaired.

In order to develop methods for removing/filtering clutter contribution, the key ingredient is to identify features that make targets different from sources of unwanted signals. Accordingly, a filter can be properly designed and tuned on clutter properties with the constraint of preserving as much as possible the useful signal which is needed for imaging purposes.

For example, in many cases, targets move. Here, the so-called moving target indicator (MTI) techniques can be employed to discern a moving target against a strong

stationary clutter. This is possible because clutter and targets have different Doppler spectra. Accordingly, a Doppler filtering is designed to cancel the zero Doppler spectral content [5]. However, there are several cases where scatterers are at rest.

In some further cases, it is known that targets have localized spatial supports, whereas sources of clutter do not. This occurs, for example, when targets are embedded in layered host media, as in subsurface or through-wall imaging. In these cases, clutter contribution mainly arises from medium interfaces whose spatial Fourier spectrum is concentrated around low frequencies. Accordingly, a high-pass filter, that suppresses the data low harmonic spatial content, can be employed to mitigate clutter [6]. Subtraction of the average trace, over sensor number, as well as the difference approach sketched in [7] in the framework of TWI, are examples of this strategy. However, filtering also erases the continuous component of the target spectral content [8]. Therefore, some compensation procedure is required to restore imaging point spread function.

Time gating does not suffer from this drawback as clutter rejection is achieve by nulling the first part of the acquired time traces [1]. Therefore, in principle, it works only in filtering out clutter that arrives before signals to be exploited for imaging.

In these cases, the choice of the time window is crucial and could be difficult if media are dispersive, as time-delayed echoes of the transmitted signal can be distorted and can extend beyond their expected duration. Moreover, multiple reflections between medium interfaces, that may occur after target backscattered field is arrived, are not eliminated. This may be the case of TWI imaging and intrawall diagnostics.

In this paper, we introduce a different time-widowing strategy to reject clutter from measurements. The starting point is the observation that the field reflected from interfaces has a strong similarity over different sensor positions, when a multimonostatic configuration is employed. Accordingly, by introducing an entropy-based measure of this similarity, signals at instants of time where entropy exceeds a prescribed threshold are nulled [9]. Note that this allows for clutter reduction also when it does not appear before the target scattered field.

The applicative context within we move is that relevant for intrawall diagnostics. In this case, targets are represented by localized inhomogeneities present within a masonry structure.

The remaining of the paper is organized as follows. In Section 2, we briefly describe the scattering experiment. In Section 3, we introduce the entropy-based clutter rejection method, whereas its numerical assessment is presented in Section 4. Finally, conclusions are drawn at the end the paper.

2. Scattering Layout

The scenario consists of a three-layered medium. The first and the third layers are assumed to be the free space with ε_0 and μ_0 being their dielectric permittivity and magnetic permeability, respectively. The second layer is representative

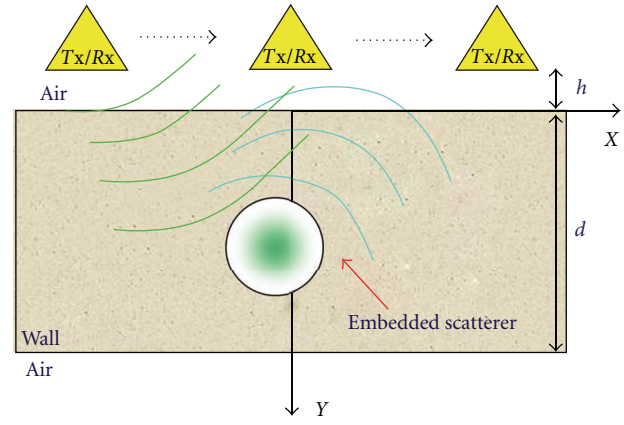

Figure 1: Geometry of the scattering problem.

of the wall. It is assumed nonmagnetic (i.e., its magnetic permeability is equal to the one of free space) with thickness d, and laterally homogeneous with relative dielectric permittivity denoted as ε_w.

The transmitting antenna is located in the first layer at a distance h from the front face of the wall. We consider a multimonostatic measurement configuration where the reflected field is collected at the same position as the source while the latter moves over a set of M different positions in order to synthesize the measurement line Σ, the latter being parallel to the wall interfaces. In particular, here, a two-dimensional filamentary current directed along the z-axis is considered as source.

Targets to be searched for reside within the wall structure and are represented in terms of spatially localized inhomogeneities. Invariance along the z-axis is assumed so that the problem at hand is two-dimensional and scalar.

The scattering layout is depicted in Figure 1. This configuration can be considered as schematizing a B-scan of the scene.

3. Entropy-Based Clutter Rejection

Let us denote as $e_1(t), e_2(t), \ldots, e_n(t), \ldots, e_M(t)$ the signals (A-scans) collected over the M observation positions. Each of them accounts for different contribution arising from antenna mismatch, from wall reflections, and from the enclosed targets. In particular, the signal collected at the nth position can be written as

$$e_n(t) = e_{na}(t) + e_{nw}(t) + e_{nt}(t), \tag{1}$$

where $e_{na}(t)$ represents the antenna internal reflection, $e_{nw}(t)$ the wall contribution, and $e_{nt}(t)$ is the field scattered by the targets within the wall (to be used for their detection and localization). Accordingly, $e_{na}(t)$ and $e_{nw}(t)$ are sources of clutter which target signals must compete with. Moreover, clutter is generally much stronger than target returns and this can make scatterer contributions barely visible or can completely mask it. Therefore, in order to "extract" $e_{nt}(t)$ from clutter, a clutter rejection method is indeed necessary.

The key steps in any clutter rejection method is to identify the features which make clutter different from the target signal, and to exploit them to suppress it from the total signal (1). Of course, these features depend on the scattering scene at hand and the nature of scatterers of interest.

When scatters with finite-spatial supports are of concern (hence, no layer interfaces), like in many subsurface or intrawall imaging problems, wall reflections and the field scattered by the targets have different spatial spectral contents. Indeed, the spectral content of the clutter due to the interfaces spans substantially the low-frequency region. Therefore, it can be mitigated by filtering out such a harmonic content [6]. The simplest way to achieve that is to subtract from each total field trace (1) the average (over the number of sensors) trace, that is,

$$e_{\mathrm{AV}n}(t) = e_n(t) - \frac{1}{M}\sum_{m=1}^{M} e_{nw}(t), \tag{2}$$

where the subscript AV on the left side term is a remind of average trace substraction. However, this filtering also acts on $e_{nt}(t)$ making it necessary for some compensation procedure in order to restore the point spread function if a focusing algorithm is employed [7].

It is observed that $e_{na}(t)$ and $e_{nw}(t)$ "precede" in time $e_{nt}(t)$. Therefore, instead of spatial frequency, difference in the time of arrival can be used to erase clutter. This suggests a time-gating procedure for clutter mitigation which does not introduce unwanted filtering. In this case, the issue to be tackled concerns the automatic selection of the window whithin which signal must be "silenced." This could become a difficult task when it is not true that "all" the clutter precedes target signal. The latter circumstance can occur, for example, when targets are embedded in a layered medium like in intrawall diagnostics. In these cases, a suitable windowing function has to be defined in order to remove clutter that appears spread at different instants of time along each A-scan trace.

To cover these situations, here, an entropy-based criterion for window selection is exploited.

The starting point is the assumption that clutter has similar behaviour in each timetrace. Note that this assumption is implicitly implied by average subtraction in (2) and even in time gating. Accordingly, the windowing function will be supported over those instants of time where trace "similarity" is "low." Of course, this statement needs to be properly cast under a "quantitative" point of view. In other words, a suitable metric has to be defined in order to quantify trace "similarity."

To this end, we first introduce the normalized A-scan as follows:

$$\widetilde{e}_n(t) = \frac{|e_n(t)|^2}{\sum_{m=1}^{M} |e_m(t)|^2}. \tag{3}$$

It is recognized that $\widetilde{e}_n(t) \geq 0$ and that $\sum_{n=1}^{M} \widetilde{e}_n(t) = 1$for all t. Therefore, for each instant of time, the vector of the normalized A-scan can be assimilated as a probability density function. Accordingly, at a given instant of time,

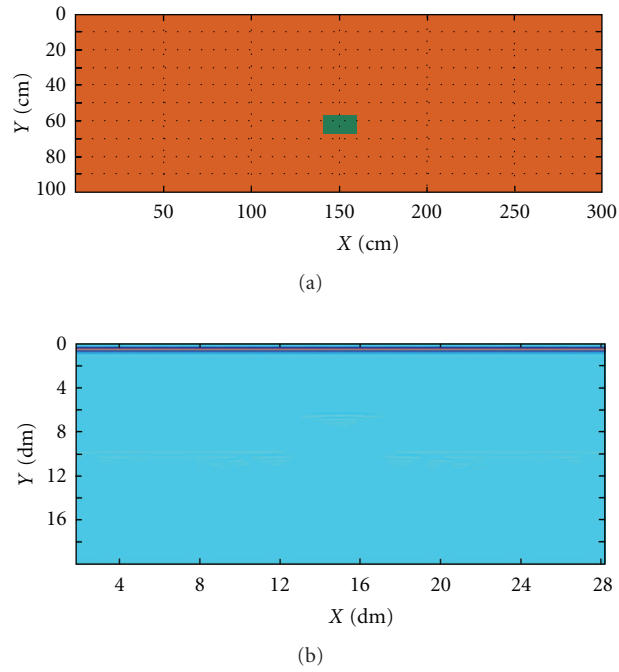

Figure 2: (a) PEC scatterer located within the wall, (b) corresponding B-scan.

similar signals (over the different sensors' positions) will translate into a uniform probability density distribution. This observation suggests to adopt an entropy-based metric in order to discriminate between clutter and target signal. Following the Shannon entropy measure, a possible choice is

$$\varepsilon_S(t) = -\sum_{n=1}^{M} \widetilde{e}_n(t)\log[\widetilde{e}_n(t)]. \tag{4}$$

As clutter signals are expected to be similar, they result in large values of $\varepsilon_S(t)$. On the contrary, target signals will consist of pulses differently delayed and hence correspond to lower value of $\varepsilon_S(t)$. Accordingly, in order to get rid clutter, a windowing, which eliminates signals for instants of time where $\varepsilon_S(t)$ is high, can be set up. Hence, one obtains the widowed signals as

$$e_{Wn}(t) = W(t)e_n(t), \tag{5}$$

with

$$W(t) = \begin{cases} 0 & \text{if } \varepsilon_S(t) = \log M \\ 1 & \text{elsewhere,} \end{cases} \tag{6}$$

where $\log M$ is the maximum of $\varepsilon_S(t)$ which occurs when all signals are identical.

Instead of Shannon entropy measure, here, we adopt a variant due to Renyi [10]. Accordingly, for quantifying the diversity between signals, we use the Renyi entropy, that is,

$$\varepsilon_{R\beta}(t) = \frac{1}{(1-\beta)\log\sum_{n=1}^{M} \widetilde{e}_n(t)^{\beta}}, \tag{7}$$

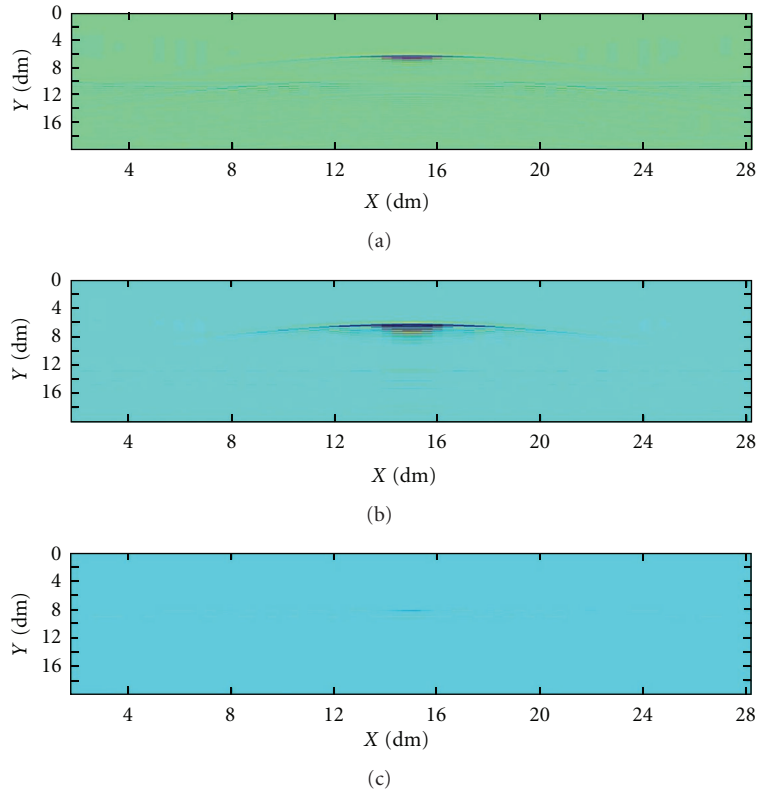

Figure 3: Windowed signal for three different values of $\widetilde{M}$. (a) $\widetilde{M} = 36$, (b) $\widetilde{M} = 10$, (c) $\widetilde{M} = 4$.

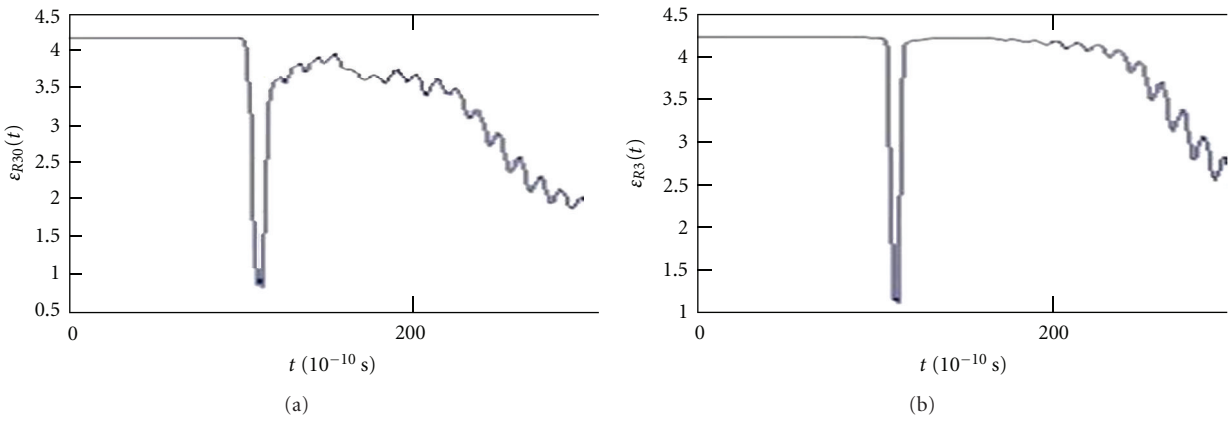

Figure 4: Renyi entropy for $\widetilde{M} = 10$ and two different values of β. (a) $\beta = 30$, (b) $\beta = 3$.

where $\varepsilon_{R\beta}(t)$ is the Renyi entropy of order β, with β being positive but different from unity. It is easily seen that Renyi entropy maximum is still $\log M$ and that it coincides with Shannon entropy for the case of $\beta = 1$. Therefore, we can conlude that, for clutter arising from antenna internal reflections and the field reflected from the front face of the masonry structure, the two entropy measures are equivalent.

However, Renyi entropy is here preferred because the exponential term β is a one more degree of freedom that can be exploited. In more detail, the contributions arriving at sensors are weighted in different way during entropy evaluation. In particular, for $\beta > 1$, Renyi entropy mainly depends on the highest "probability events" (highest $\widetilde{e}_n(t)$). Therefore, a "sharper" separation between clutter and target signals is expected.

Eventually, the window function to be used is defined as follows:

$$W(t) = \begin{cases} 0 & \text{if } \varepsilon_{R\beta}(t) \geq \alpha \log M \\ 1 & \text{elsewhere,} \end{cases} \tag{8}$$

with $\alpha < 1$. Note that a decision threshold lower than $\log M$ has been introduced this way, it is expected that back wall face reflections and multiple target echoes are mitigated as well. In fact, multiple target echoes appear in the radargramm (B-scan) as hyperbolas whose radii of curvature are greater than the ones of the target signals. This is because they can be regarded as due to scatterers that are more deeply located. On the other hand, their radii of curvature are certainly smaller than the interface reflections which appear as flat curves. Hence, entropy associated to those returns will be greater than that due to the target but lower than the one due to wall interfaces.

4. Numerical Examples

In this section, the ability of the windowing procedure described above to remove clutter is checked. To this end, a series of numerical experiment are conducted with synthetic data obtained by using the FDTD-based GPRMAX forward solver [11].

As source, a filamentary impressed current located over ($h = 0$) the front face of the wall is employed. Sixty-six source positions (i.e., $M = 66$) uniformly taken over a measurement line $3m$ long are considered. The field is collected at the same position as the source as the latter spans the measurement line. It is worth noting that, in this case, as ideal source is considered, $e_{na}(t) = 0$. Hence, clutter solely arises from the masonry structure.

As to the wall, a slab with thickness $d = 1$ m and dielectric permittivity $\varepsilon_w = 7$ is considered. Such a wall resembles to some hancient walls in Italy [12].

4.1. Choice of β and α. The first set of numerical examples have the aim of providing a guide for the choice of the parameters β and α appearing in (7) and (8), respectively.

To this end, we consider a single rectangular perfect electric conducting (PEC) scatterer embedded in the masonry structure, as depicted in Figure 2, and apply different windowing function as β and α vary. For comparison purposes, in Figure 2, it is also reported the radargramm corresponding to the scattering experiment at hand. In particular, depth is provided in terms of $y = vt/2$, where v is wave propagation speed in the wall.

First, for the fixed value of $\beta = 3$, the role of α is studied in Figure 3, where the windowed $e_W(t)$ data are reported for three different values of α. In particular, α is chosen so that $\widetilde{M} = \exp(\alpha \log M)$ is equal to 36, 10, and 4, respectively, from the top to the bottom panels. Of course, cases corresponding to $\widetilde{M} > M$ do not make any sense as entropy measure would be always lower than the windowing threshold and hence signal would remain unchanged. According to (8), the lower $\widetilde{M}$, the stronger the windowing since the threshold above which signal is silenced is lower. This is clearly shown in Figure 3. In particular, it can be appreciated that, in all the cases, first wall interface contribution is successfully erased. This makes it evident target contribution, which otherwise would be only barely visible in the radargramm (see Figure 2). Moreover, as expected, by decreasing the windowing threshold, also artifacts due, basically, to the second wall interface, tend to be erased. However, a too low threshold would cancel target contribution as well.

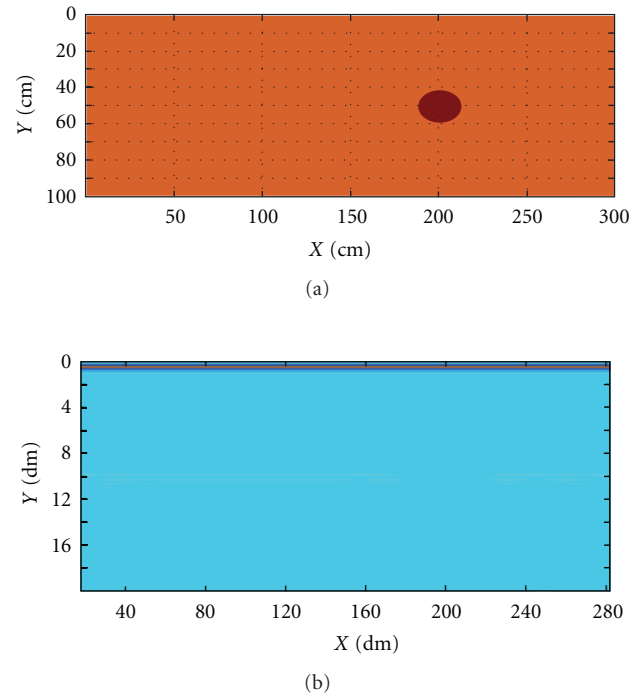

Figure 5: (a) Circular dielectric scatterer located within the wall, (b) corresponding B-scan.

Therefore, according to these results, a judicious choice appears $\widetilde{M} = 10$.

With this value of $\widetilde{M}$, we turn now to address the role of β by referring to Figure 4. In such a figure, Renyi entropy is reported for two different values of β ($\beta = 30$ and $\beta = 3$) for a time interval which roughly corresponds to the depth range of Figures 2 and 3. As can be seen, the first part of entropy behavior is rather constant and approximately equal to the maximum value $\log M = 4.2$. This of course could be expected as, in this interval of time, there is a strong similarity between different A-scans which mainly account for front wall reflections. Moreover, it is observed that entropy abruptly drops at around 10.5 ns and stays down roughly for a time interval corresponding to the round-trip delays that signals take to cover antenna/target paths and vice versa. Afterwards, entropy starts to increases once again.

However, entropy measures is a slowly varying function of β as the two entropy behaviors are very similar (as shown in Figure 4).

Therefore, according to this numerical analysis, in the sequel we set $\beta = 3$ and $\widetilde{M} = 10$.

5. Numerical Results

In this section, we check the entropy windowing procedure for scattering scenes different from the one reported in Figure 2 which, in turn, guided the choice of β and $\widetilde{M}$. In particular, while the wall structure remains the same as

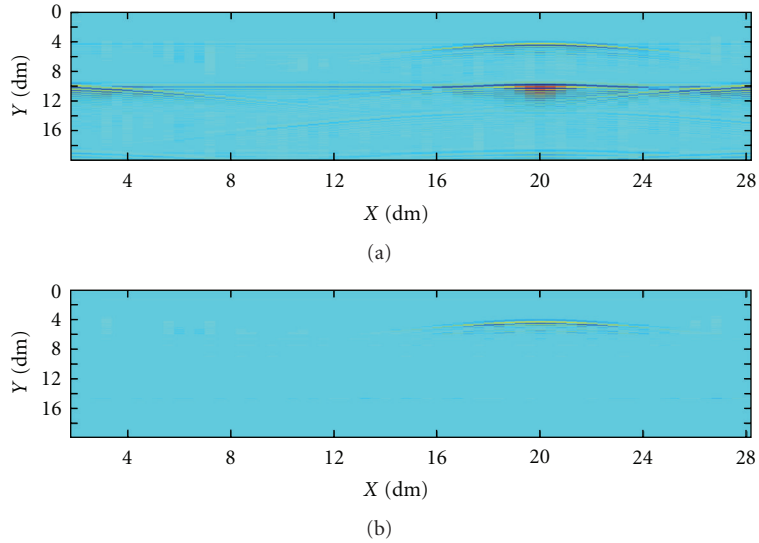

Figure 6: The case of Figure 5. (a) Radargramm after average trace subtraction, (b) windowed radargramm.

the previous case, the type of scatterers and their positions are changed.

The first example refers to the scattering scene reported in Figure 5, where a circular dielectric scatterer with relative dielectric permittivity equal to 4 and electric conductivity of 0.1 S/m is considered. Also, its location within the wall, which is different from the case reported in Figure 2, is indicated. In the same figure (Figure 5(b)) the corresponding radargramm is reported as well.

By looking at such a figure, it can be appreciated that target can be hardly discerned from background. Indeed, one could be aware of the presence of a scatterer mainly due to the shadowing that it introduces on the reflection coming from second wall interface. Instead, after windowing (see Figure 6(b)), target contribution turns to be clearly visible.

In the same figure, we also reported, for comparison purposes, the radargramm after average trace subtraction according to (2). By comparing the two methods, it is seen that in both cases, front wall interface clutter is very well cancelled. However, entropy-based windowing outperforms average trace subtraction as a number of spurious artifacts, still affecting radargramm after average trace removing, are almost completely eliminated. This makes the interpretation of the windowed images less ambiguous.

As a second example, the scattering scene depicted in Figure 7 is considered. Now, two scatterers are embedded in the wall. One is circular with relative dielectric permittivity equal to 3 (in order to increase contrast with background) and electric conductivity of 0.1 S/m; the other is a PEC square. Their dimensions and positions within the wall are illustrated in Figure 7(a). In Figure 7(b), the corresponding radargramm is reported. It can be seen that the two scatterers are only barely discernable. After clutter is removed, they turn to be clearly visible, specially by the windowing procedure that, as in the previous case, allows for obtaining a more clear image (see Figure 8).

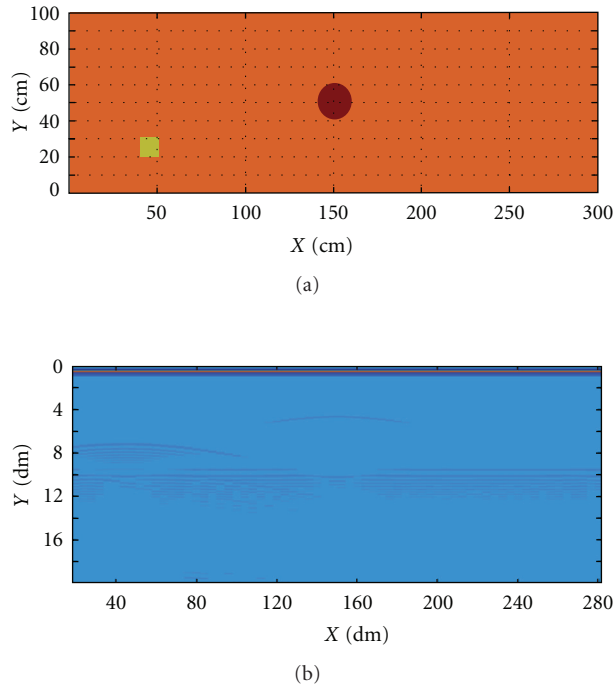

Figure 7: (a) Two scatterers are located within the wall, (b) corresponding B-scan.

6. Conclusions

In this paper, we considered intrawall diagnostics of localized scatterers and focused on the problem of clutter mitigation To this end, we employed an entropy-based time-windowing artifact removal algorithm. In particular, we exploited the fact that wall contributions give rise to signals that have high similarity over different sensors' positions. Therefore, by computing the entropy of time traces at each instant of time, a windowing function was set up so that it takes values

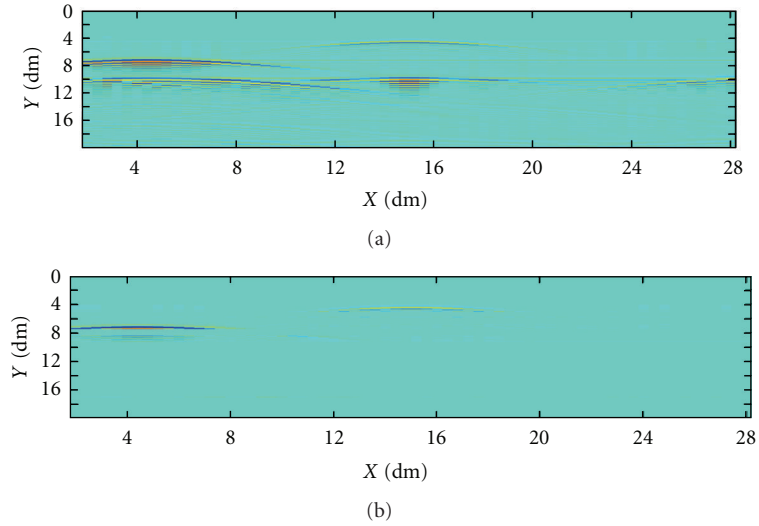

Figure 8: The case of Figure 7. (a) Radargramm after average trace subtraction, (b) windowed radargramm.

of zero for entropy greater than a suitable threshold and values of one when smaller entropy occurs.

Applying the window function to FDTD-simulated data, it was shown the effectiveness of the method. In particular, the windowing strategy proven to be more effective than standard average trace subtraction.

Although the presented results are encouraging, a more deep analysis still has to be performed. This would require a more extensive numerical investigation for different and possibly more realistic scenarios.

It is our commitment to address this study in future works.

References

[1] D. J. Daniels, Ground Penetrating Radar, IET, 2004.

[2] E. C. Fear, P. M. Meaney, and M. A. Stuchly, "Microwaves for breast cancer detection?" *IEEE Potentials*, vol. 22, no. 1, pp. 12–18, 2003.

[3] M. Amin and K. Sarabandi, "Special issue on remote sensing of building interior," *IEEE Transactions on Geoscience and Remote Sensing*, vol. 47, no. 5, pp. 1267–1268, 2009.

[4] F. Soldovieri and R. Solimene, "Ground Penetrating Radar subsurface imaging of buried objects," in *Radar Technology*, G. Kouemou, Ed., In-Tech, 2010.

[5] N. Levanon, *Radar Principles*, John Wiley & Sons, New York, NY, USA, 1988.

[6] D. Potin, E. Duflos, and P. Vanheeghe, "Land mines ground-penetrating radar signal enhancement by digital filtering," *IEEE Transactions on Geoscience and Remote Sensing*, vol. 44, no. 9, pp. 2393–2406, 2006.

[7] M. Dehmollaian, M. Thiel, and K. Sarabandi, "Through-the-wall imaging using differential SAR," *IEEE Transactions on Geoscience and Remote Sensing*, vol. 47, no. 5, pp. 1289–1296, 2009.

[8] R. Persico and F. Soldovieri, "A microwave tomography approach for a differential configuration in GPR prospecting," *IEEE Transactions on Antennas and Propagation*, vol. 54, no. 11, pp. 3541–3548, 2006.

[9] W. Zhi and F. Chin, "Entropy-based time window for artifact removal in UWB imaging of breast cancer detection," *IEEE Signal Processing Letters*, vol. 13, no. 10, pp. 585–588, 2006.

[10] R. G. Baraniuk, P. Flandrin, A. J. E. M. Janssen, and O. J. J. Michel, "Measuring time-frequency information content using the Rényi entropies," *IEEE Transactions on Information Theory*, vol. 47, no. 4, pp. 1391–1409, 2001.

[11] A. Giannopoulos, GprMax2D/3D, Users Guide, 2002, http://www.xmarks.com/site/www.gprmax.org/.

[12] A. Brancaccio, R. Solimene, G. Prisco, G. Leone, and R. Pierri, "Intra-wall diagnostics via a microwave tomographic approach," *Journal of Geophysics and Engineering*, vol. 8, pp. 47–53, 2011.